ELSEVIER

Contents lists available at ScienceDirect

Acta Biomaterialia

journal homepage: www.elsevier.com/locate/actabiomat



Full length article

Endowing polyetheretherketone with synergistic bactericidal effects and improved osteogenic ability



Jianglong Yan ^a, Wenhao Zhou ^a, Zhaojun Jia ^{a,d}, Pan Xiong ^a, Yangyang Li ^a, Pei Wang ^a, Qiyao Li ^b, Yan Cheng ^{a,*}, Yufeng Zheng ^{a,c}

- ^a Academy for Advanced Interdisciplinary Studies, Peking University, Beijing 100871, China
- Department of Biomedical Engineering, Materials Research Institute, Huck Institutes of The Life Sciences, The Pennsylvania State University, University Park, PA 16802, USA
- ^c Department of Advanced Materials and Nanotechnology, College of Engineering, Peking University, Beijing 100871, China
- d Department of Orthopaedic and Traumatology, The University of Hong Kong, 21 Sassoon Road, Pokfulam, Hong Kong, China

ARTICLE INFO

Article history: Received 8 May 2018 Received in revised form 23 August 2018 Accepted 29 August 2018 Available online 31 August 2018

Keywords: Polyetheretherketone Synergistic bactericidal Osteogenic pH-responsive

ABSTRACT

Biomedical associated infections (BAI) are difficult to treat and may even lead to amputation and death, especially after the emergence of drug-resistant bacteria. The aim of this study was to harness the potential synergistic effects of multiple bactericidal agents to endow polyetheretherketone (PEEK) with the ability of achieving full eradication of planktonic and adherent bacteria while maintaining acceptable biocompatibility. In this work, a mussel inspired, silver nanoparticles (AgNPs) incorporated silk fibroin (SF)/gentamicin sulfate (GS) coating was constructed upon porous PEEK surface. The obtained coating greatly enhanced the bactericidal efficiency to Gram-positive bacteria and Gram-negative bacteria. The number of bacteria survived in the culture medium after treated with this coating was 10⁶ fold lower than that survived after treated with PEEK sample, while the number of viable bacteria adhered to this coating was 10⁵ lower than that adhered to PEEK sample. Furthermore, release of Ag* and GS increased with decreasing pH, indicating great potential of this coating to be a "smart" bacteria-triggered self-defensive coating. Meanwhile, this functional coating shows favorable cytocompatibility and osteogenic ability. The mechanism behind this dual function is also partially revealed. Expectedly, this "smart" dual function coating can give a promise for PEEK to become a solution to increasingly deteriorated BAI.

Statement of Significance

In this study, a mussel inspired, silver nanoparticles (AgNPs) incorporated silk fibroin (SF)/gentamicin sulfate (GS) coating was constructed upon porous polyetheretherketone (PEEK) surface. This design was aimed to provide a solution to the increasingly deteriorated biomedical associated infections (BAI). Actually, this design endowed PEEK with dual function: bacteria-triggered synergistic bactericidal effect and improved osteogenic ability. The combination of silver and GS exhibited synergistic bacteria killing effect on both Gram-positive and Gram-negative bacteria, which showed 10⁶ times higher in releasing-killing and 10⁵ times higher in anti-adhesion than that of untreated PEEK. Furthermore, release of bactericidal agents increased with decreasing pH, indicating great potential of this coating to be a bacteria-triggered self-defensive coating. More interestingly, this study revealed the mechanism of synergistic effect between silver and GS.

© 2018 Acta Materialia Inc. Published by Elsevier Ltd. All rights reserved.

1. Introduction

Biomedical device-associated infections (BAI) has been a crucial issue accounting for 3% of failures of medical devices [1,2]. It causes delayed healing, implant failures, and repeated surgeries [3–5]. Meanwhile, it can lead to increased hospitalization times and treatment costs, the requirement for implant removal and tissue debridement, and high morbidity and in worst cases even

^{*} Corresponding author.

E-mail address: chengyan@pku.edu.cn (Y. Cheng).

death [6]. Additionally, these issues have become even more prevalent with the increasing use of biomaterial implants.

To deal with this situation, antibiotics have been widely used in surgeries. However, the abuse of antibiotics has led to the emergence of bacterial resistance, which has become a serious problem in public health. For this reason, silver has been considered as one of the most promising candidates, as it has been a common disinfectant for several millennia because of its strong toxicity to a wide range of micro-organisms [7]. It also has been showed to possess the capability to perturb different pathways of cell metabolism [8,9], for which bacterial can hardly develop resistance. However, bacteria with silver resistance still appeared [10,11]. Therefore, it's urgent for us to find a new way to kill bacteria efficiently while without the appearance of bacteria resistance. Currently, Ag+ has been proved to be synergistic with antibiotics to potentiate antibacterial activity significantly and even to expand the antibacterial spectrum [12]. For this reason, constructing a system on biomedical devices to achieve on-demand simultaneous release of Ag⁺ and antibiotics would be a better choice, and these biomedical devices would be a promising candidate for orthopedic implantation.

Gentamicin sulfate (GS), as one antibiotic has been widely used in orthopedic surgery for its broad-spectrum action against many strains, was chosen in this work [13]. In another aspect, polyetheretherketone (PEEK) has been considered as a prospective material for orthopedic implantation, due to its elastic modulus close to cortical bone's and excellent chemical resistance [14]. Furthermore, PEEK has many other advantages, such as good sterilization resistance, wear resistance, natural radiolucency and magnetic resonance imaging (MRI) compatibility [15]. However, its antibacterial property is inferior to titanium [16], which limits the application of PEEK, and can result in bacterial infection [17]. For this reason, it appears necessary to improve the antibacterial properties of PEEK. Surface modification can be a good choice to enhance the surface biological properties while maintaining the superior properties of the materials.

In this study, a combination coating of silver and GS was applied to modify the surface of PEEK. Silver was in the form of silver nanoparticles (AgNPs), because they are a reservoir of Ag⁺ so as to control the release of Ag⁺ while maintaining a higher concentration of Ag⁺ in specific area for a long time [18]. AgNPs can be introduced onto the substrate through many different approaches [19], but a mussel-inspired self-polymerized polydopamine (PDA) was

employed for the following reasons. First, PDA can reduce Ag⁺ into AgNPs, and firmly anchored it onto PEEK surface [20], which would achieve a long-term antibacterial effect and potentially relieve the concerns about the toxicity of AgNPs for mammalian cells and bodies. Second, PDA has been reported to be biocompatible which would be a benefit to osteogenesis [21].

In order to incorporate GS, silk fibroin (SF) was utilized. It possesses positive charges under physiological environment (isoelectric point (pl) is about 4.2), which facilitates the loading of GS because of the electrostatic interaction between positively charged SF and negatively charged GS. What's more, the electric charge and molecular conformation of SF can vary with pH, which can lead to pH responsive controlled release of GS [22,23]. In addition, SF shows good biocompatibility both in vitro and in vivo, which is crucial to the success of implantation [24,25].

More specifically, a three-dimensional (3D) porous structure was introduced into PEEK surface via sulfonation treatment [17,26], for the sake of stronger adhesive force with PDA. The application of PDA can not only anchor AgNPs but also can be a bridge between the underlying PEEK and SF/GS [27,28]. In this study, it's the first time to achieve a PDA assisted in situ growth of AgNPs and immobilization of SF/GS coating upon porous PEEK surface (Fig. 1), and the details of sample names are summarized in Table S1. The efficacy of the designed antimicrobial hybrid was assessed in vitro against *Staphylococcus aureus* (*S. aureus*) and *Escherichia coli* (*E. coli*), and the osteogenesis performance was evaluated using mouse osteoblastic cells (MC3T3-E1). In addition, the mechanism underlying the antimicrobial complex's enhanced killing effect was elucidated.

2. Experimental section

2.1. Sample preparation

Medical grade PEEK materials were machined into a disc shape with dimensions of $\Phi15\times1.5~mm^3.$ All the samples were mechanically polished to mirror finish followed by ultrasonically washed in acetone, ethanol, and deionized (DI) water sequentially.

2.2. Preparation of silk fibroin

Silk fibroin stock solution was prepared as previously described [29]. Briefly, cocoons of *Bombyx mori* (*B. mori*) were boiled for

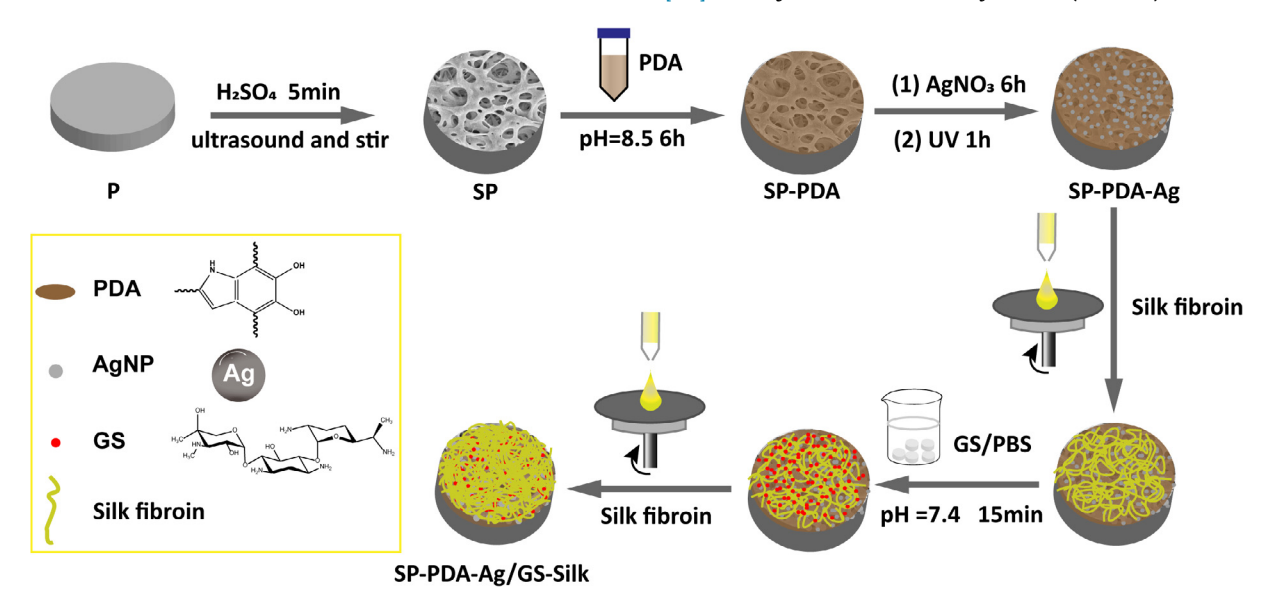


Fig. 1. Illustrative diagrams for surface functionalization of PEEK by polydopamine assisted silk-based AgNPs/gentamicin coating.

30 min in an aqueous solution of $0.02~M~Na_2CO_3$ and then rinsed thoroughly with deionized water to remove the glue-like sericin proteins. The extracted silk fibroin was then dissolved in 9.3~M~LiBr solution at 60~C~for~4~h, yielding a 20%~(w/v) solution. This solution was dialyzed against DI water using a dialysis bag (MEMBRA-CEL, 12,000-14,000~MWCO) at room temperature for 48~h~to remove the salt. The dialysate was centrifuged twice at 4~C~for~20~min, in order to eliminate the impurities. The final concentration of silk fibroin solution was about 7-8%~(wt/vol).

2.3. Surface functionalization of PEEK

The strategy to functionalize the surface of PEEK is depicted in Fig. 1. First, sulfonation treatment was applied to obtain a 3D uniform porous network structure. It was conducted in sulfuric acid (95–98 wt%, Aldrich Chemical Corp) under the condition of ultrasound and stir at room temperature for 5 min. After that, the sulfonated samples were taken out and ultrasonically rinsed in DI water to remove the residues on the surface. Then 4 h of hydrothermal treatment at 100 °C was conducted followed by rinsed with DI water and dried at room temperature (SP). Secondly, a mussel-inspired strategy to immobilize AgNPs onto the surface of SP was applied. The SP samples were subjected into 2 mg/mL dopamine hydrochloride (Aladdin) in Tris-HCl buffer (10 mM, pH = 8.5; Sigma) for 6 h under constant vibration in darkness at 37 °C, then ultrasonically washed in Tris-HCl buffer to detach excess monomer and particles (SP-PDA). Further, the SP-PDA samples were immersed in AgNO₃ (0.5 mM; Beijing Chemical Reagent Co., Ltd., China) solution for another 6 h, and then exposed to ultraviolet for 1 h (UV, $\lambda = 254$ nm, 2.5 W/m²) to further reduce AgNPs (SP-PDA-Ag). Finally, the silk and gentamicin were introduced onto SP-PDA-Ag surface together. Three layers of silk were spun onto the surface of SP-PDA-Ag, then SP-PDA-Ag samples were immersed into the solution of gentamicin (500 µg/mL in PBS) for 15 min followed by the coating of another three silk layers (SP-PDA-Ag/GS-Silk).

2.4. Surface characterization

Field-emission scanning electron microscopy (FE-SEM, Hitachi S-4800, Japan) was employed to examine the surface morphology and microstructure of the prepared specimens, and the pore size distribution was calculated by the freeware ImageJ. For composition analysis, X-ray photoelectron spectroscopy (XPS, Kratos, UK), and microscopic Fourier transform infrared spectroscopy (Micro-FTIR, Thermo Fisher) were employed. The surface hydrophilicity of the samples was determined by water contact angle measurements (Kino, USA) at ambient humidity and temperature.

2.5. Ag⁺ release into phosphate buffer solution (PBS)

To examine the release behavior of Ag^+ , specimens (SP-PDA-Ag and SP-PDA-Ag-Silk) (n = 3) were immersed in 2 mL of PBS with different pH (pH = 4.5, 5.0, 7.4) at 37 °C in darkness for 28 days. The entire volume of solution was collected and refilled with fresh PBS at predetermined time points (1 h, 3 h, 6 h, 12 h, 24 h, 2 d, 5 d, 7 d, 10 d, 14 d, 21 d, 28 d). Then, the inductively coupled plasma-atomic emission spectrometer (ICP-MS, Agilent 7700, USA) was used to determine the release profiles and rates of Ag^+ .

2.6. Release of gentamicin sulfate (GS) in different pH of PBS

To investigate the pH-responsive release behavior of gentamicin, specimens (SP-PDA-Ag/GS-Silk) (n=3) were immersed in 2 mL of PBS with different pH (pH = 4.2, 5.0, 7.4) at 37 °C in darkness for 4 weeks. Then the entire volume was collected at predeter-

mined time points (1 h, 3 h, 6 h, 12 h, 24 h, 2 d, 5 d, 7 d, 10 d, 14 d, 21 d, 28 d), and fresh PBS was refilled accordingly. All of these collected solutions were filtered using an Ultra Centrifugal Filter Units (Millipore, USA) to remove the silk fibroin. Then the concentration of gentamicin was measured using o-phthaldialdehyde (OPA), as described elsewhere [30]. The mixture's fluorescence, which were used to determine the release profile and release rate of gentamicin, were read using a Shimadzu UV-3600 PLUS spectrophotometer at 257 nm.

2.7. Protein adsorption

Bovine serum albumin (BSA, 1 mg/mL) was used for the protein adsorption investigation. Aliquots of 500 μ L were transferred onto each sample in 24-well plates (TCPS, Corning, USA), and incubated at 37 °C for 2 h. Subsequently, samples were washed with fresh PBS to remove the nonadherent protein, followed by co-culture with sodium dodecyl sulfate (SDS, 2%) with shaking at 37 °C for 2 h. Quantitatively, optical density (OD) at 570 was determined on a microplate reader (Bio-RAD, USA) through the employment of a Micro BCA Protein Assay Reagent Kit (Thermo Scientific).

2.8. Antibacterial assay

The antibacterial ability of the prepared samples against grampositive *S. aureus* (ATCC, 25923) and gram-negative *E. coli* (ATCC 25922) was determined by the plate-counting method. The bacteria cultured in the Luria Bertani (LB) medium was diluted into 1.0×10^5 colony forming units (CFU)/mL), then 1 mL of this bacterial suspension was added to the sterilized samples followed by incubating at 37 °C for 1 d, 3 d, 5 d, and 7 d. At the end of each incubation period, the viable bacteria in the suspension were quantified by standard serial dilution and plate-counting. As to the viable bacteria adhered to the samples, it was determined by plate-counting method after samples were rinsed in PBS and ultrasonically for 10 min.

2.9. SEM observation of bacterial morphology

E. coli and *S. aureus* cells were incubated with different samples for 24 h. The samples were then gently washed with PBS to remove non-adherent bacteria. Afterward, the adherent bacteria on samples were fixed with 2.5% glutaraldehyde overnight followed by dehydrating in graded ethanol, SEM was applied to observe the bacterial morphology.

2.10. Membrane permeability measurements

The sodium dodecyl sulfate (SDS) can be used to monitor membrane permeability, because it is difficult to penetrate an intact membrane but more likely to penetrate the destabilized cell membrane. The measurement of bacterial membrane permeability by SDS has been mentioned before [31]. In brief, *E. coli* and *S. aureus* cells were cultured with different samples in the LB medium at 37 °C for 3 h. Then the bacterial suspension was centrifuged to remove the medium and the same volume of medium was added. Finally, SDS (0.1% concentration) was added followed by the monitor of OD₅₇₀.

2.11. Production of reactive oxygen species (ROS) within per bacteria

The production of ROS was quantified by DCFH-DA assay (Reactive Oxygen Species Assay Kit, cat# E004; Nan-jing-jian-cheng, China). Briefly, *E. coli* and *S. aureus* cells at a final concentration of 10^5 CFU/mL were incubated with $10~\mu M$ of DCFH-DA and samples at $37~\rm ^{\circ}C$ for $3~\rm h$. The number of viable bacteria in each suspen-

sion was measured through the spread plate test method. After that, the bacterial suspension was centrifuged to collect the viable bacteria, then the same volume of PBS was added. The level of cellular ROS was measured as the relative fluorescence intensity, which was detected by fluorescence spectrophotometer (FL-3-22, HORIBA) in fluorescence mode with excitation at 488 nm and emission at 525 nm. Meanwhile, the standard curve of the concentration of ROS could be acquired by using several concentrations of ROS standard samples. Under the help of the standard curve and bacterial number in each suspension, we can quantify the ROS production in each bacterium.

2.12. The ROS quenching experiment

ROS can be reduced through the addition of thiourea, an ROS scavenger. This test has been mentioned before [12]. In brief, each bacterium (*E. coli* or *S. aureus*) at a concentration of 10^5 CFU/mL was incubated with each sample at 37 °C for 24 h, simultaneously with addition of thiourea (150 mM). For the CFU measurement, $100~\mu L$ of culture was collected and then serially diluted in PBS for proper multiples. A $100~\mu L$ portion of each dilution was plated in LB-agar plates and incubated overnight at 37 °C. The colonies were counted, and CFU/mL was calculated.

2.13. Cell culture

Mouse pre-osteoblast cells (MC3T3-E1) were cultured in Dulbecco's modified eagle's medium (DMEM, Gibco) supplemented with 10% fetal bovine serum (FBS, Gibco) and 1% penicillin/streptomycin (HyClone, USA) in a humidified atmosphere of 5% $\rm CO_2$ at 37 °C. When 80–90% confluence was reached, cells were harvested by mild trypsinization, centrifugation, resuspended and diluted to the desired density in the complete culture medium. The medium was refreshed every 2 days.

2.14. Cell proliferation and morphology

To assess the cell proliferation, the Cell Viability Kit (CCK-8, Dojindo, Japan) was employed. Briefly, The MC3T3-E1 cells were seeded on each sample at a density of 5×10^4 cells per well in 24-well plates and cultured for 3, 5, and 7 days. At the end of each time point, the samples were transferred to a new 24-well culture plate. The incubation medium containing 10% CCK-8 was then added and incubated at 37 °C for 1.5 h. Afterwards, 100 μL of the reaction solution was transferred into a new 96-well plate, and the absorbance was read at the wavelength of 450 nm by a microplate reader.

To investigate cell morphology, MC3T3-E1 pre-osteoblasts were seeded on each sample in 24-well plates at a density of 5×10^4 cells per well. After incubating for 6 h and 24 h, the samples were rinsed twice with PBS. Then the cells on the samples were fixed with 2.5% (v/v) glutaraldehyde in PBS at 4 °C overnight followed by dehydrated in graded ethanol for SEM observation.

2.15. Osteogenic differentiation studies

To determine the early differentiation of MC3T3-E1 preosteoblasts on samples, cells were seeded on samples in 24-well plates at a density of 5×10^4 cells per well. After incubation for 7 and 14 days, ALP staining was performed according to the manufacturer's instructions (Nan-jing-jian-cheng, China). Briefly, the cells on the specimens were lysed in 1% Triton X-100 for 1 h, and p-nitrophenyl phosphate (p-NPP) was added into cell lysis. After incubation at 37 °C for 15 min, the optical density of each sample was measured at 520 nm, and ALP activities were calculated by extrapolation from a standard curve. The ALP levels were normal-

ized to the total protein content and described as U per gram of protein.

The collagen secretion and extracellular matrix (ECM) mineralization assays were carried out after 5×10^4 cells/well were seeded on the samples in 24-well plates at 37 °C for 28 d. For the degree of collagen secretion, specimens were fixed in 4% paraformaldehyde (PFA) for 15 min followed by staining with 0.1% solution of Sirius Red (Sigma) in saturated picric acid overnight. Afterwards, specimens were thoroughly rinsed with 0.1 M acetic acid, and optic images for each sample were acquired. Quantitatively, the stain was eluted in 400 µL of the destain solution (0.2 M NaOH/methanol 1:1) followed by the measurement of optic density at 570 nm using a microplate reader. To investigate the ECM mineralization, specimens were stained with Alizarin Red S (ARS, Sigma; 2%, pH = 4.3) for 10 min at 4 °C before rinsed with DI water to eliminate unbound stain. Then optical images were acquired. Afterwards, the bound Ca was dissolved using 10% cetylpyridinium chloride for 2 h and the absorbance of the resulting solution was measured at 562 nm.

2.16. Statistical analysis

Three samples were used in each group, and the results were expressed as mean \pm standard deviations. One-way analysis of variance (ANOVA) or Student's-test was used to measure the statistically significant difference (p) among groups, and a p value <0.05 was considered to be statistically significant.

3. Results

3.1. Surface characterization

The surface morphologies were observed by SEM (Fig. 2a). After sulfonation treatment, the originally smooth morphology was changed into a three dimensional (3D) network porous structure. The obtained micrographs were analyzed with Imagel software which revealed that most of the pores were between 1.0 and 2.0 µm in diameter (Fig. 2b). Subsequently, the resulting surfaces were immersed into a dopamine solution to form the PDA layer. Owing to the nanoscale reactive nature of PDA [32], the porous morphology of SP was kept, forming a thin island-shaped film. Further, the resultant samples were impregnated into silver nitrate solution, which led to in situ growth of AgNPs. One more step of UV exposure was applied to thoroughly reduce the remained silver ions. Consequently, uniform and densely packed AgNPs (~60 nm) were formed on the surface. Ultimately, silk fibroin was spun onto the surface, which can incorporate gentamicin through the electrostatic interactions.

Fig. 2c shows the FTIR spectra acquired from the PEEK control. In both the PEEK and SP samples, all the characteristic bands were present. The peaks at 1651, 1489 and 926 cm⁻¹ were related to the diphenylketone, which exists in the structure of PEEK [33]. The C-O-C stretching vibration of the diaryl group was evident at 1187 and 1159 cm⁻¹, whereas the peak at 1595 cm⁻¹ corresponded to the C=C in the benzene ring [26]. However, closer examination revealed characteristic polymer bands from SP-the peaks at 1255 cm⁻¹ and 1055 cm⁻¹, which were correlated to the dissymmetric stretching vibrations of O=S=O and the symmetric stretch of S=O, respectively [34]. In the sample of SP-PDA-Ag/GSsilk, two new strong absorptions peaks appeared at 1648 and 1537 cm⁻¹, which corresponded to the characteristic amide I and amide II, respective [35]. This data confirm the existence of silk fibroin on the surface. In order to further verify the element composition, XPS was employed. From the XPS survey spectra (Fig. 2d), characteristic elements of each sample were found, and the atomic

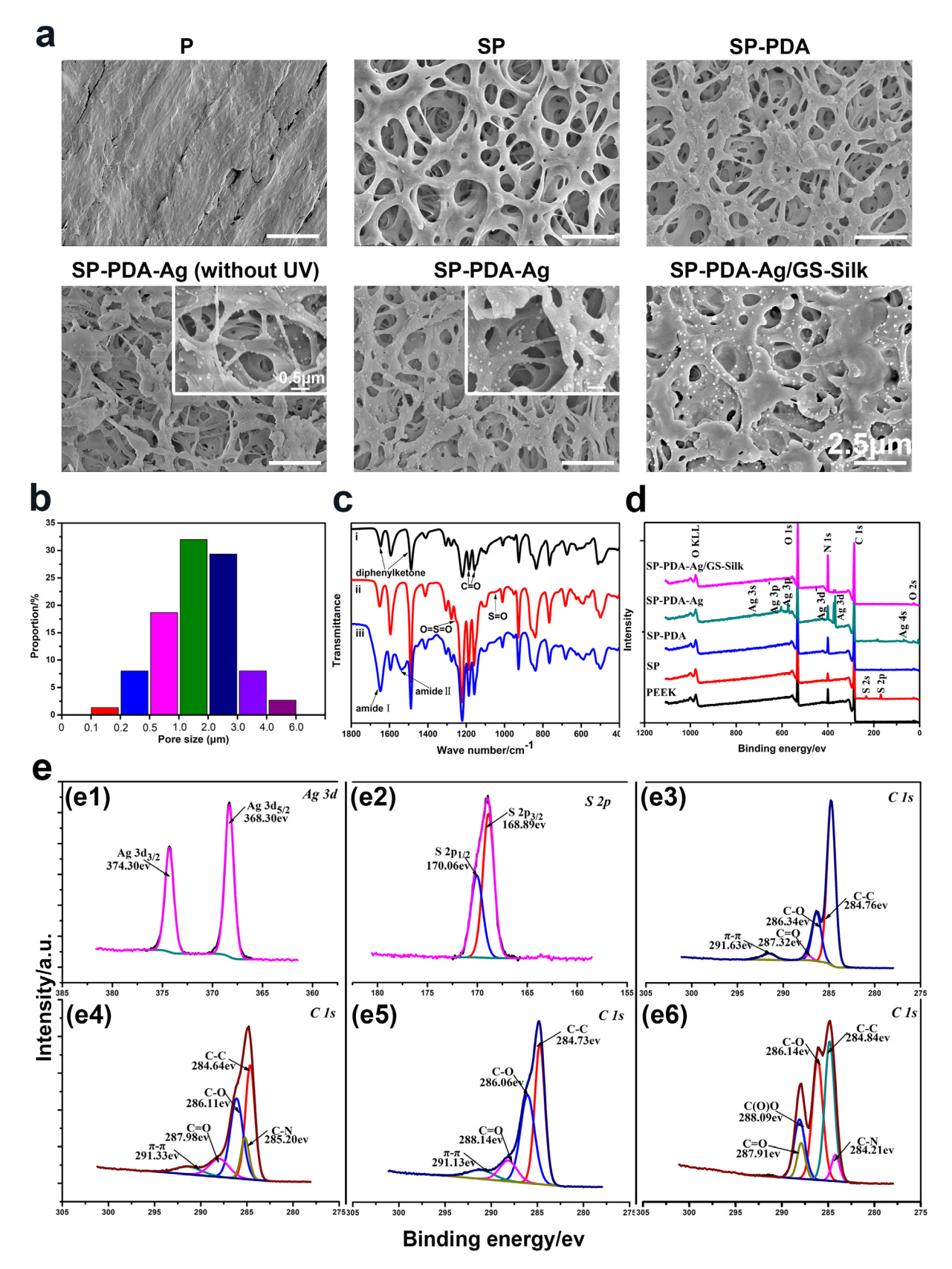


Fig. 2. (a) Surface morphology of various samples. (b) Diameter distribution of micro/nano pores of SP analyzed by ImageJ software. Chemical composition of the coatings: (c) FTIR spectra of (i) PEEK, (ii) SP, (iii) SP-PDA-Ag/GS-silk; (d) Survey spectra of XPS; and (e) high resolution XPS spectra of (e1) Ag 3d from SP-PDA-Ag, (e2) S 2p from SP, and (e3-6) C 1 s from SP, SP-PDA, SP-PDA-Ag and SP-PDA-Ag/GS-silk, respectively.

concentrations were listed in Table 1. The appearance of sulfur signal in SP sample at 168.89 and 170.06 eV corresponded to S 2p_{3/2} and S $2p_{1/2}$ with a high oxidation state, which indicated the existence of SO₃H group and was in accordance with the result from FTIR spectra [36]. After PDA deposition, the concentration of nitrogen increased from 3.07% to 6.65%, which was due to the higher content of nitrogen in PDA. What's more, the N/C ratio was 0.088, close to the theoretically N/C ratio-0.125 of PDA. Compared with Fig. 2e3, the appearance of binding energy at 285.2 eV was due to the C-N group in PDA (Fig. 2e4), which further confirmed PDA was formed on the PEEK surface. Furthermore, 368.3 and 374.3 eV binding energies corroborated Ag (0) $3d_{5/2}$ and Ag (0) 3d_{3/2}, respectively (Fig. 2e1), which indicated the existence of AgNPs upon the SP-PDA-Ag sample. Besides, the disappearance of sulfur and silver signals (Fig. 2d) with the increase of nitrogen concentration (Table 1) on the surface of SP-PDA-Ag/GS-Silk could be ascribed to the silk fibroin coatings. Meanwhile, the highresolution C 1 s spectra of SP-PDA-Ag and SP-PDA-Ag/GS-silk were compared (Fig. 2e5, e6), where the peak at 288.09 eV was due to the carboxyl group in silk, further revealing the success deposition of silk.

3.2. Release of gentamicin and Ag+

The release profiles of Ag^+ and GS were displayed in Fig. 3. The total Ag content for both samples with and without silk films were $6\pm0.3~\mu g$. Compared with the release behavior of Ag^+ controlled by PDA, the additional layers of silk fibroin further slowed down the release rate (Fig. 3a, Fig. S1). It is noteworthy that the silk showed a pH-responsive behavior to the release of Ag^+ . After 28 d, only 10.7% (644 ng) of Ag^+ was leached into PBS at pH 7.4, while 38.9% (2332.8 ng) and 32% (1923.3 ng) of Ag^+ was released at pH 4.5 and 5.0, respectively. For GS, the release rate and release amount were much higher when exposed to acidic environment (pH = 4.5, 5.0), compared with physiological pH (Fig. 3b). At different pH conditions, GS exhibited sustained release performances in the first 14 d. Later, the release rate of GS increased dramatically over time, especially under acidic environment, owing to the degradation of silk film.

3.3. Hydrophilicity

The static water contact angles (CA) were determined by the sessile water drop, in order to evaluate the hydrophilicity of the modified surface (Fig. S2a). The contact angle for PEEK was about 65° whereas that value was increased to 81° after sulfonation treatment. On the other side, the PDA coating decreased the CA to 49° while the deposition of silver did not change the CA too much (46°). However, the CA of SP-PDA-Ag/GS-Silk sample increased to 56°.

3.4. Protein adsorption

The protein adsorption capacity of biomaterials has important influences on cell attachment. Fig. S2b displayed the amount of protein adsorbed on different samples, which were: SP-PDA-Ag/

GS-silk > SP-PDA-Ag > SP-PDA > SP > PEEK. Obviously, PDA and silk fibroin played a significant role in the improvement of protein adsorption ability.

3.5. Antibacterial assessment and SEM observation

Bacterial infections played a critical role in the failure of medical device implantation. Bactericidal and anti-adhesion are the pivotal properties for biomaterials to fight against bacterial infections. In this study, the releasing-killing and anti-adhesion activities of each coating were evaluated by samples cultured with S. aureus or E. coli, which represent Gram-positive and Gram-negative bacteria, respectively. During the first 24 h, the incorporation of AgNPs or GS alone did not improve antibacterial (both release-killing and anti-adhesion) activity significantly. However, the combination of AgNPs and GS greatly enhanced the inhibitory effect on the growth of both S. aureus and E. coli, which showed the number of survived bacteria after treated with SP-PDA-Ag/GS-Silk samples were 10⁶ fold lower in release-killing and 10⁵ fold lower in antiadhesion than that after treated with P samples (Fig. 4). What's interesting, the SP samples with porous structure showed better anti-bacterial adhesion property than pure PEEK samples for E. coli. As to the long-term antibacterial assay, the SP-PDA-Ag/GS-Silk group also performed reliable antibacterial ability against S. aureus and E. coli (Fig. S3). For the other group, the bacteria reached a maximum number at 3 d and later began to decline. This may result from the lack of nutrition in the medium.

SEM was employed to further explore the anti-adhesion ability of the coatings (Fig. 5). It clearly showed that bacteria adhered to, proliferated and aggregated on P, SP, and SP-PDA with smooth and intact cell membrane, and most of them undergo the binary or multiple fission process. It is noteworthy that a large number of *S. aureus* bacteria inhabited inside the porous structure of SP, which could lead to implant failure. On the contrary, the SP-PDA-Ag or SP-PDA-GS-Silk sample reduced the amount of adhered bacteria, and distorted or even destroyed the structure of bacteria as indicated in Fig. 5 (the red arrows). Furthermore, no bacteria were witnessed on the coating with the combination of AgNPs and GS.

3.6. Membrane permeability

SDS was used to determine whether the functional coatings affected the integrity of the outer membrane of bacteria because the destabilization of membrane leads to an increased susceptibility to SDS, and would lead to decrease in the bacteria turbidity (OD $_{570}$). Fig. 6a, b displayed that the OD $_{570}$ values of pure PEEK, SP, and SP-PDA were lower than the control group (bacteria cultured alone) at the initial 1.5 h, which meant pure PEEK, SP, and SP-PDA had adverse effects on the bacteria membrane compared with the control group. Whereas, at the 3 h point, the OD $_{570}$ values of bacteria grown on these coatings were higher than the control group, which indicated the bacteria was in a better condition when grown on these coatings. On the other hand, both the coatings with AgNPs or GS decreased the OD $_{570}$ values compared with control group at any determined time points, and the coating employed AgNPs presented much lower of OD $_{570}$ value than the coating

Table 1Concentration of the elemental composition on the surfaces of the functionalized coating as determined by XPS.

Samples/Elements (At.%)	С	0	N	S	Ag
PEEK	80.87	13.87	5.26	0	0
SP	77.25	17.74	3.07	1.93	0
SP-PDA	75.36	17.77	6.65	0.23	0
SP-PDA-Ag	73.57	17.80	6.65	0	1.98
SP-PDA-Ag/GS-Silk	66.13	17.62	16.20	0	0.05

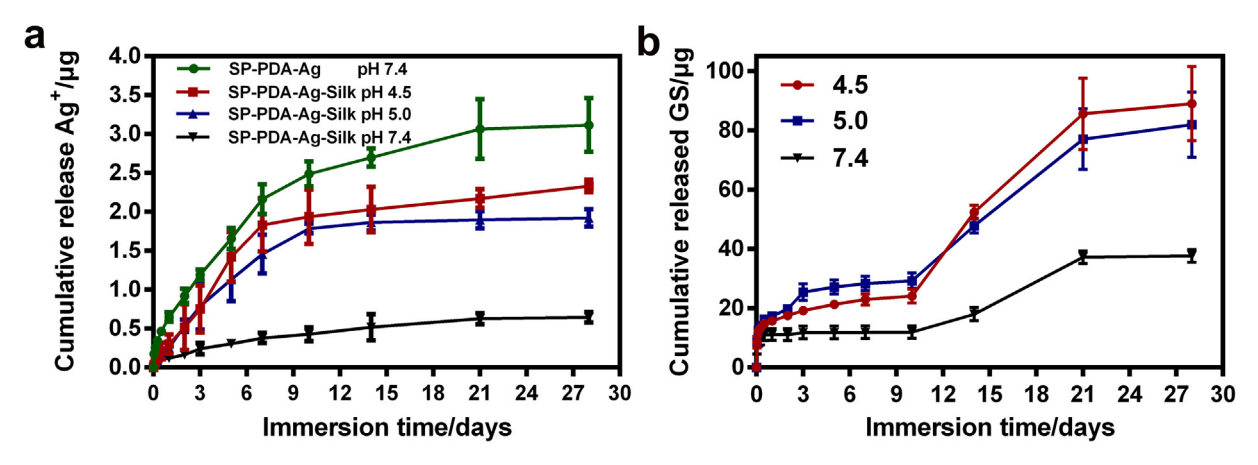


Fig. 3. The release behavior of silver in (a) cumulative release amount, and the release behavior of GS from SP-PDA-Ag/GS-Silk samples in (b) cumulative release amount.

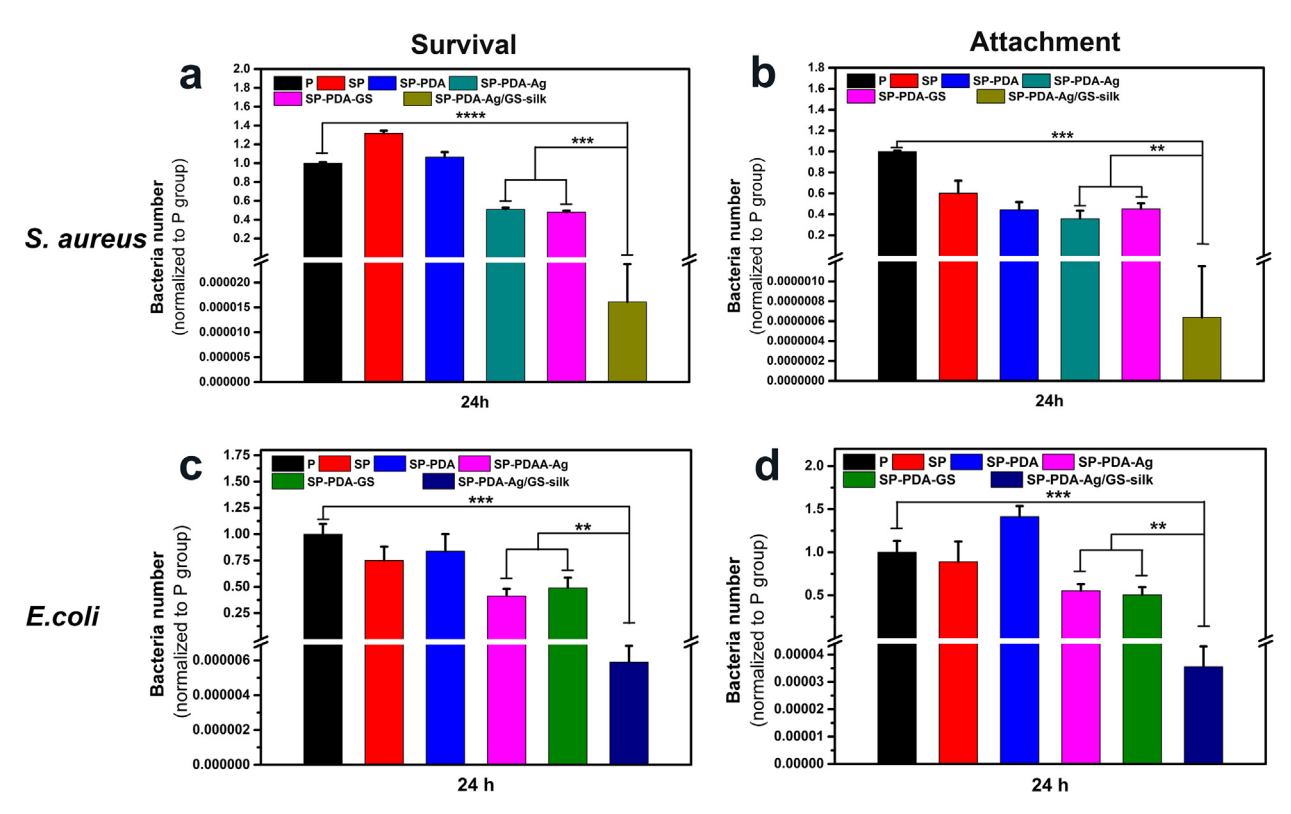


Fig. 4. Antibacterial activities of different samples against both *S. aureus* and *E. coli* for 24 h. The number of (a) *S. aureus* and (c) *E. coli* survived in the culture medium after treated with different samples normalized to that survived after treated with P sample, and the number of viable (b) *S. aureus* and (d) *E. coli* adhered to different samples normalized to that adhered to P sample. *P < 0.05; **P < 0.01; ****P < 0.001; ****P < 0.0001.

employed GS at both time points, suggested that AgNPs had a stronger ability to rupture bacteria membrane. It is noteworthy that the combination of AgNPs and GS did not show a significant synergistic effect in lowering the OD₅₇₀ value compared with AgNPs alone, which indicated the combination of AgNPs and GS only mildly improved the ability to destroy the bacteria membrane.

3.7. Production of ROS within per bacteria

Excess production of ROS may be a common mechanism of cell death [37]. The production of ROS within per bacteria was represented in Fig. 6c, d. It illustrated that, when compared with PEEK, AgNPs potentiated the production of ROS about 15 times and 17

times for *S. aureus* and *E. coli*, respectively; while GS only had slightly influence in the production of ROS. However, the combination of AgNPs and GS greatly increased ROS production, which was 10^3 times higher than that of PEEK.

3.8. The quenching of ROS

The addition of thiourea eliminated the adverse effects of ROS, and the corresponding results were given in Fig. 6e, f. Compared with PEEK samples, both SP and SP-PDA exhibited several times of increasement in the number of viable bacteria for both *S. aureus* and *E. coli*, which indicated improved bacterial survival and growth. As to AgNPs or GS, the number of viable bacteria for both *S. aureus* and *E. coli* was reduced, even without the destructive

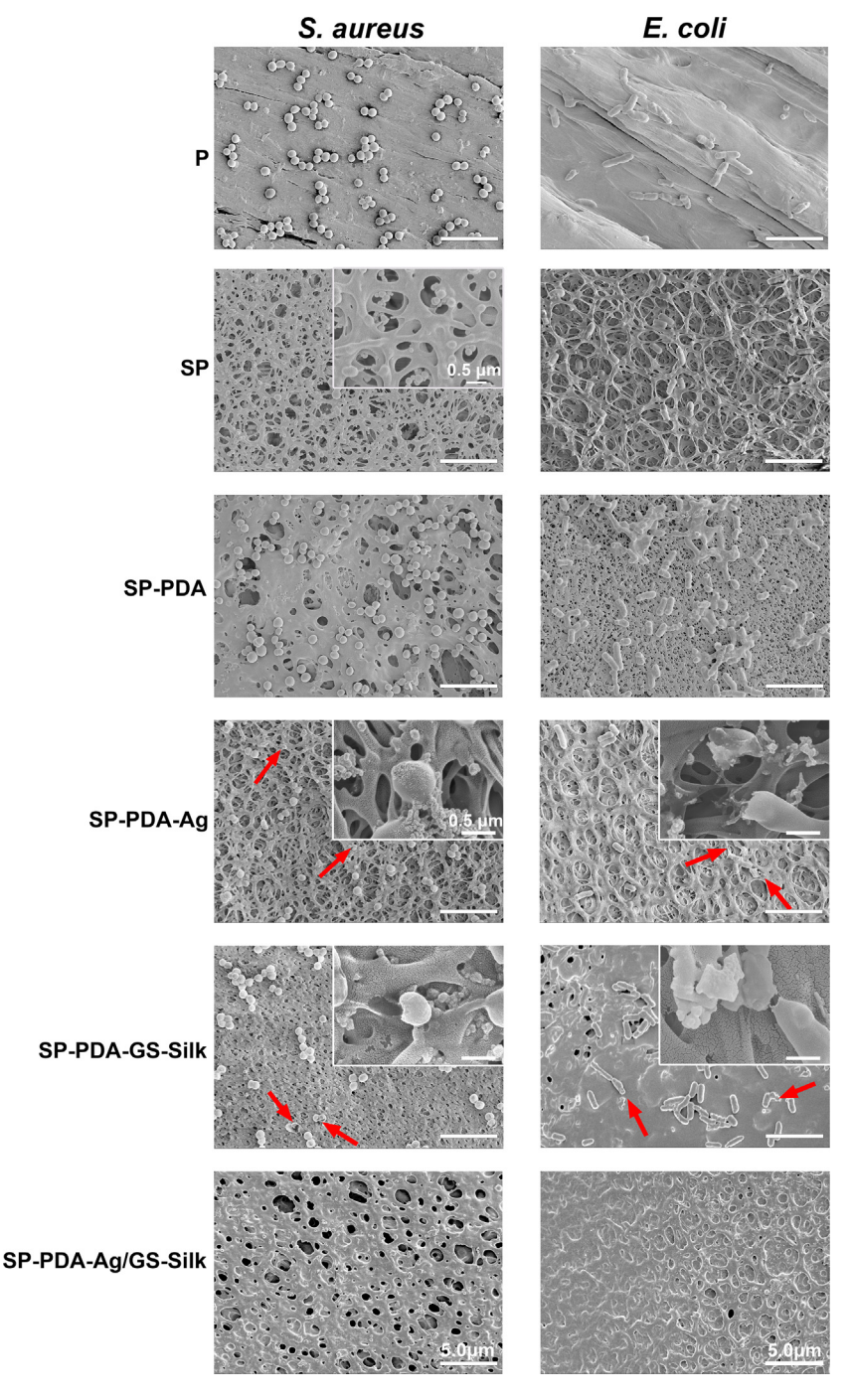


Fig. 5. SEM morphology of bacteria adhered to the surfaces after incubated with samples for 24 h, and high magnification images of bacteria adhered to SP sample or bacteria damaged were inserted on the upper right corner. Red arrows indicate bacteria with impaired structure. (For interpretation of the references to color in this figure legend, the reader is referred to the web version of this article.)

effect of ROS. Furthermore, under the combination of AgNPs and GS, the majority of *S. aureus* and *E. coli* was killed, only about 1% of them was still alive.

3.9. Cytocompatibility evaluation

To investigate the effects of different coatings on the cell attachment, SEM was employed to observe cells at the determined time points. After 6 h cultivation, as detailed in Fig. 7, cells adhered on the PEEK surface appeared a spherical shape with few microvilli

and thinly spread filopodium-like morphology. On the contrary, the porous and PDA coatings enable cells to adhere in flatter morphologies with lamellipodia outstretching to sense the substrate. However, the existence of AgNPs inhibited the adhesion of cells. Luckily, on the SP-PDA-Ag/GS-silk surface, the adherent cells presented elongated configuration with cytoplasmic projections stretching toward the surface. Nonetheless, it was too early for them to fully spread out. In comparison, after 24 h, the cells displayed more extensively spread cytoplasm on all the surfaces than those at 6 h. Specifically, the SP-PDA-Ag/GS-silk surface showed a

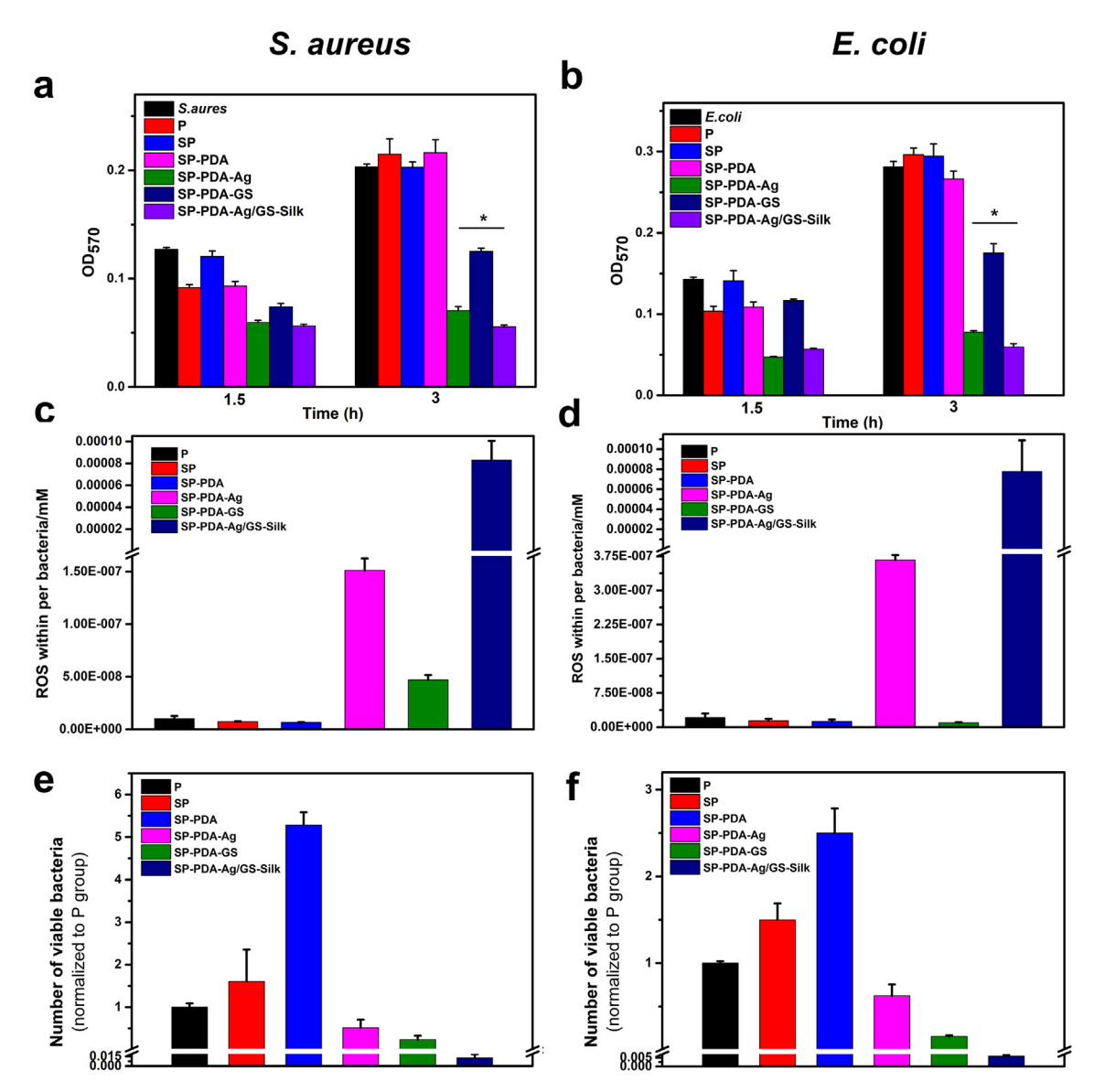


Fig. 6. Membrane permeability of (a) *S. aureus* and (b) *E. coli* treated with SDS after incubated with different samples for 3 h, were measured by microplate reader at the wavelength of 570 nm. *P < 0.05. Production of ROS within per (c) *S. aureus* and (d) *E. coli* bacteria cell after co-cultured with different samples for 3 h. (e) *S. aureus* and (f) *E. coli* were incubated with different samples for 24 h with the addition of thiourea, the number of viable bacteria in the culture medium were normalized to that of P group.

greater cell number, and some of the cells were already sub-confluent. This revealed that the SP-PDA-Ag/GS-silk sample had no deleterious effect on cell adhesion and spreading.

The proliferation of cells was measured according to the CCK-8 method. Compared with the negative group, the PEEK showed inferior cytocompatibility, while the porous structure favored the cell proliferation at every time point (Fig. 8a). However, the presence of AgNPs showed deleterious effect on cell proliferation, which could be ascribed to the release of Ag*. The existence of silk film favored cells' proliferation.

3.10. Osteogenic differentiation properties

As an early marker for cell differentiation, ALP activity was determined. As detailed in Fig. 8b, the ALP activity for all group increased from 7 d to 14 d. The ALP activity of cells cultured on SP-PDA-Ag presented to be the lowest at both determined time points, disclosing the negative effect of AgNPs on the osteo-differentiation ability of cells. Nevertheless, the ALP activity expression on SP-PDA-Ag/GS-silk coating was higher than that of

PEEK at 7 d and 14 d. To further investigate the osteogenic capability, Sirius red and ARS staining were applied to estimate the collagen secretion and extracellular matrix mineralization abilities, because they are osteogenic markers at a later stage. The SP-PDA-Ag/GS-Silk coating exhibited the largest staining area and deepest red color for both Sirius red and ARS staining, which suggested the highest osteo-differentiation activity (Fig. 8e). In addition, quantitative analysis was carried out, and the results corresponded with aforementioned staining results (Fig. 8c, d). Generally speaking, the presence of AgNPs and GS in the SP-PDA-Ag/GS-silk coating did not show adverse effect on osteo-differentiation, and on the contrary, the coating promoted cell osteogenesis compared with the untreated PEEK.

4. Discussion

Morones-Ramirez et al. [12] have founded that the combination of Ag⁺ and antibiotics could result in a significant synergistic effect on killing the drug-resistant bacterial strains, thereby expanding

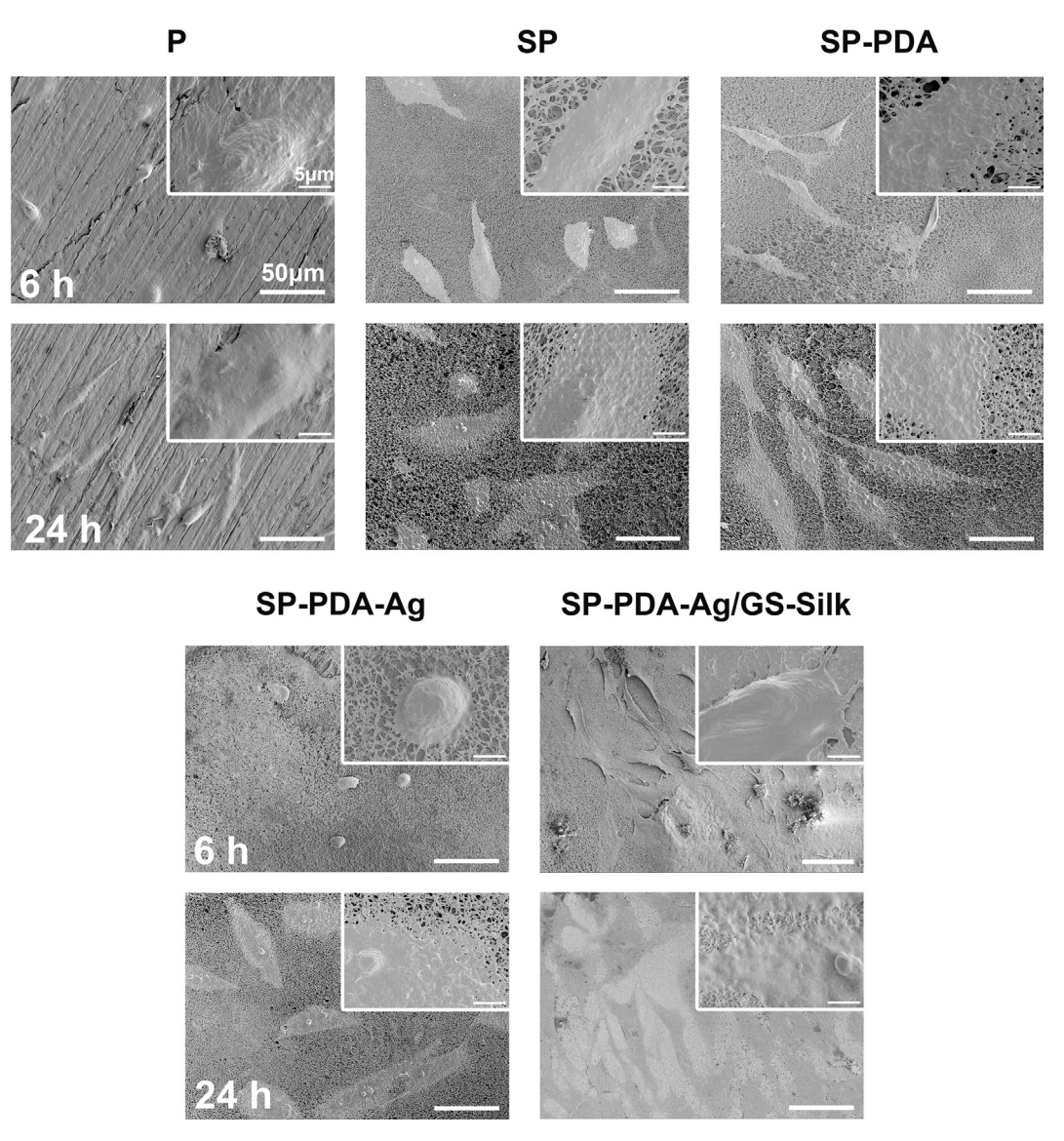


Fig. 7. Morphology of MC3T3 cells after cultured on different samples for 6 h and 24 h.

the antibacterial spectrum of the existing antibiotics. Since then, some studies have explored the possibility of integrating the synergistic bacterial-killing ability of Ag⁺ and antibiotics into biomedical devices [28,38,39]. Whereas, the imbalanced biocompatibility and antimicrobial properties limit their applications, while the uncontrolled release of bactericides exacerbates the emergence of bacterial resistance. Therefore, PDA and silk fibroin were introduced to the porous PEEK surface to balance biocompatibility and antibacterial ability of PEEK implant. Meanwhile, silk fibroin had the ability to control the release of bactericide, which can inhibit the emergence of bacterial resistance. As to antibacterial ability, the employed of AgNPs and GS fully eradicated both the planktonic and adherent S. aureus and E. coli bacterial even after a week incubation, while the incorporation of AgNPs or GS alone did not present prominent bactericidal ability (Fig. 4 and Fig. S3). At the first 24 h, the SP samples with porous structure showed better antibacteria adhesion property than pure PEEK samples for E. coli, which mainly attributed to two aspects. First, the incorporation of sulfur into PEEK after sulfonation showed bactericidal effect [17]. Second, the smaller surface pore size (\sim 1 μm) as compared with the size of E. coli (1-3 μm) reduced bacteria contact area [40]. Besides that, the PDA coating exhibited different influence

on the bacterial adhesion ability, owing to the different hydrophilicity of S. aureus (72°) and E. coli (\sim 20°) [41,42]. It was also noteworthy that the synergistic effect between AgNPs and GS on planktonic bacterial was 10 times higher than the effect on adherent bacteria. That could be explained by the greater difficulty in the eradication of adherent bacteria [38]. However, it seemed to be abnormal that SP-PDA-Ag did not display enhanced antibacterial properties as immobilized AgNPs on biomaterials via PDA had been reported to improve antibacterial properties [32]. This phenomenon could be explained by the amount of released Ag^+ (0.65 ± 0.06 µg after 24 h) which was far below the MIC of Ag^+ (4 $\mu g/ml$) [43]. Hence even the local concentration of Ag⁺ around the surface could not be high enough to engender significant anti-adhesion effect. On the other hand, the mechanism behind the synergistic effect of AgNPs and GS need further exploration.

The antibacterial effect of AgNPs originates from its released Ag⁺ [44], and Ag⁺ has been known to kill bacteria through membrane damage, production of ROS, and causing cellular uptake of Ag⁺ [45]. Therefore, we reasoned that AgNPs could potentiate the antibacterial ability of GS as they share a common antibacterial mechanism which involving membrane damage and overproduc-

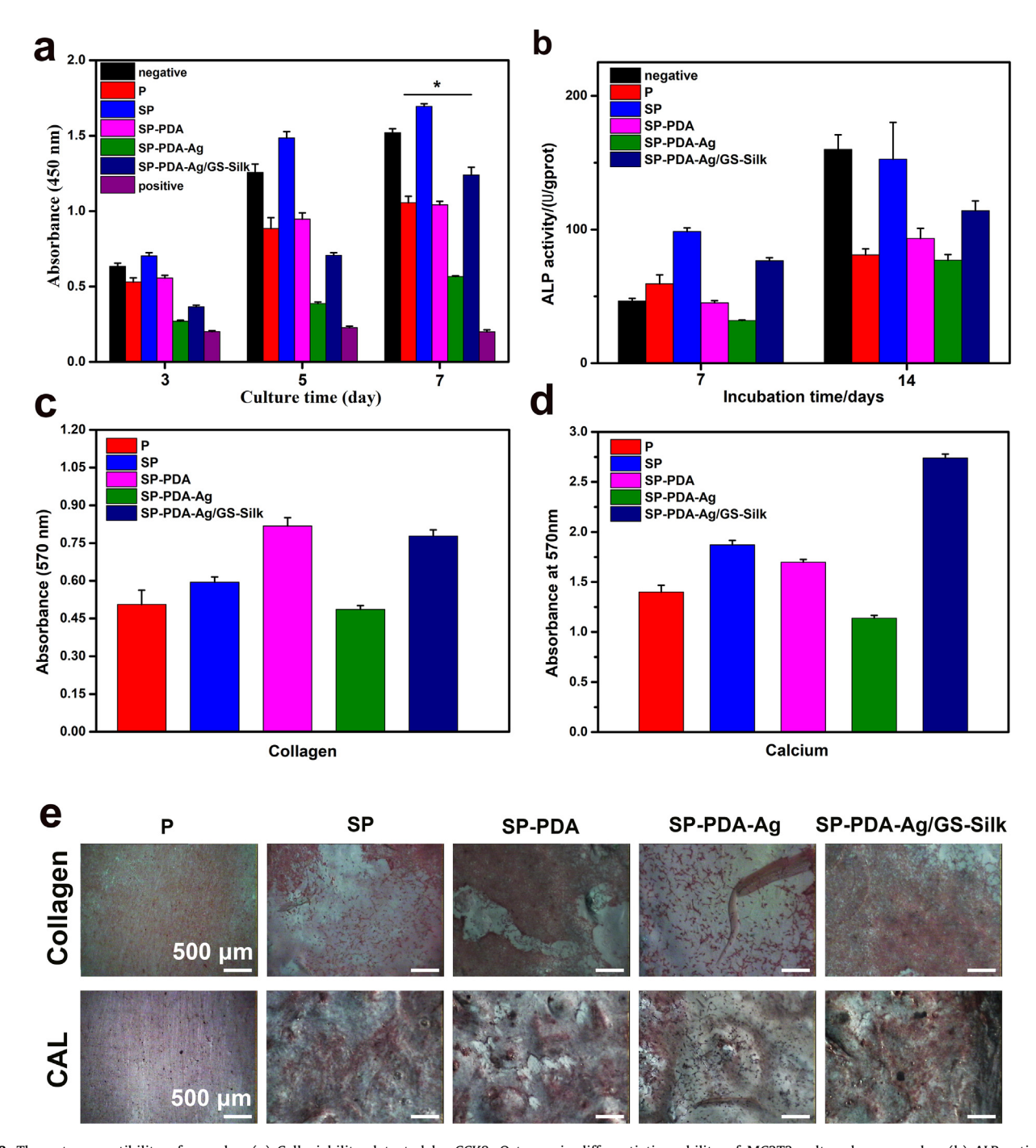


Fig. 8. The cytocompatibility of samples. (a) Cell viability detected by CCK8. Osteogenic differentiation ability of MC3T3 cultured on samples. (b) ALP activity; the quantification of (c) collagen secretion and (d) calcium deposition; (e) the coloration of collagen secretion (purplish red) and calcium (CAL) deposition (red or purplish red) on different samples for 28 d. (For interpretation of the references to color in this figure legend, the reader is referred to the web version of this article.)

tion of ROS [46,47]. In that point, membrane permeability was determined, and both AgNPs or GS showed improved bacteria membrane permeability compared with the P group, but the degree of improvement to S. aureus and E. coli was different. The E. coli exhibited greater membrane vulnerability than S. aureus when treatment with AgNPs, whereas GS treatment showed an reverse result (Fig. 6a, b). That may associate to the facts that the thicker negatively charged peptidoglycan of S. aureus can trap more silver than E. coli does, so as to decrease the membrane susceptibility of S. aureus [48]; whilst Gram-negative bacterial (E. coli) are intrinsically less permeable to GS compared with Grampositive species (S. aureus), as their outer membrane forms a per-

meability barrier [49,50]. As to sample with AgNPs/GS, it displayed the highest membrane permeability compared with the other samples. It was mainly because that Ag⁺ formed complexes with GS which led to an increase of overall surface charge [51], and the negatively charged bacteria would prefer to interact with the enhanced positively charged silver-GS complexes when compared with silver ion or GS.

As the silver-GS complex led to enhanced bacterial membrane permeability, we hypothesized that more Ag⁺ and GS can enter bacteria, yielding a locally high concentration of Ag⁺ and GS within bacteria. The localized Ag⁺ and GS can disrupt the intracellular regulation pathways of ROS or facilitate the catalytic process that

could produce ROS [8,52], leading to an increased production of ROS. Actually, the AgNPs/GS showed 10³ times increase in the ROS production of individual bacteria compared with PEEK (Fig. 6c, d), which was in line with our hypothesis. To ascertain the role of ROS in elevating bactericidal ability, bacterial activity was measured after the scavenge of ROS by thiourea. The result displayed that the number of bacteria survived after treated with SP-PDA-Ag/GS-Silk sample was 1% of that survived after treated with PEEK sample. This may originate from the DNA damage, protein inactivation, and interruption of protein synthesis, as caused by the locally high concentration of Ag⁺ and GS. This result indicated the importance of the DNA and protein damage caused by locally concentrated Ag⁺ and GS in bacterial killing, while alleviated the importance of ROS in bacterial killing.

Concluded from the abovementioned results, the potential mechanisms of synergistic effect between AgNPs and GS were considered to include increasing the bacteria membrane permeability, boosting the production of cellular ROS, and causing damage to DNA and protein (Fig. 9b). More specifically, Ag⁺ released from anchored AgNPs and formed complex with GS, as GS contains many active amino and hydroxyl groups that can react easily with Ag⁺ by chelation. These complexes were more positively charged, led to a heightened tendency of interaction with negatively

charged bacteria. Therefore, more Ag⁺ and GS were allowed to exist in close proximity to the bacteria membrane, interact and efficiently disturb the membrane. That yielded localized and more concentrated Ag⁺ and GS within bacteria. These concentrated Ag⁺ and GS contributed to bacterial-killing in two different ways: (1) Ag+ has a high affinity for amines, phosphates, and especially the thiol group, so it can bind to DNA, protein or cofactors, disturbing simultaneously many aspects of cell metabolism and resulting in bacteria death. Meanwhile, GS can bind to the 30S subunit of the bacterial ribosome irreversibly, so as to interrupt protein synthesis, and finally leading to bacterial death [53]. (2) The localized Ag⁺ and GS together can dramatically increase the cellular production of ROS through scavenging intracellular reductase enzymes to disrupt the ROS-regulation and through boosting the catalytic processes that produce ROS. One widely accepted pathway to boost the catalvtic process which produce ROS is that the existence of Ag⁺ and GS stimulate oxidation of NADH via the electron transport chain that is dependent upon the TCA cycle, hyperactivation of the electron transport chain stimulates superoxide formation, and superoxide damages iron-sulfur clusters, making ferrous irons available for oxidation by the Fenton reaction that can lead to ROS formation [47]. The evolved ROS can damage DNA, protein, and lipids, triggering bacterial death.

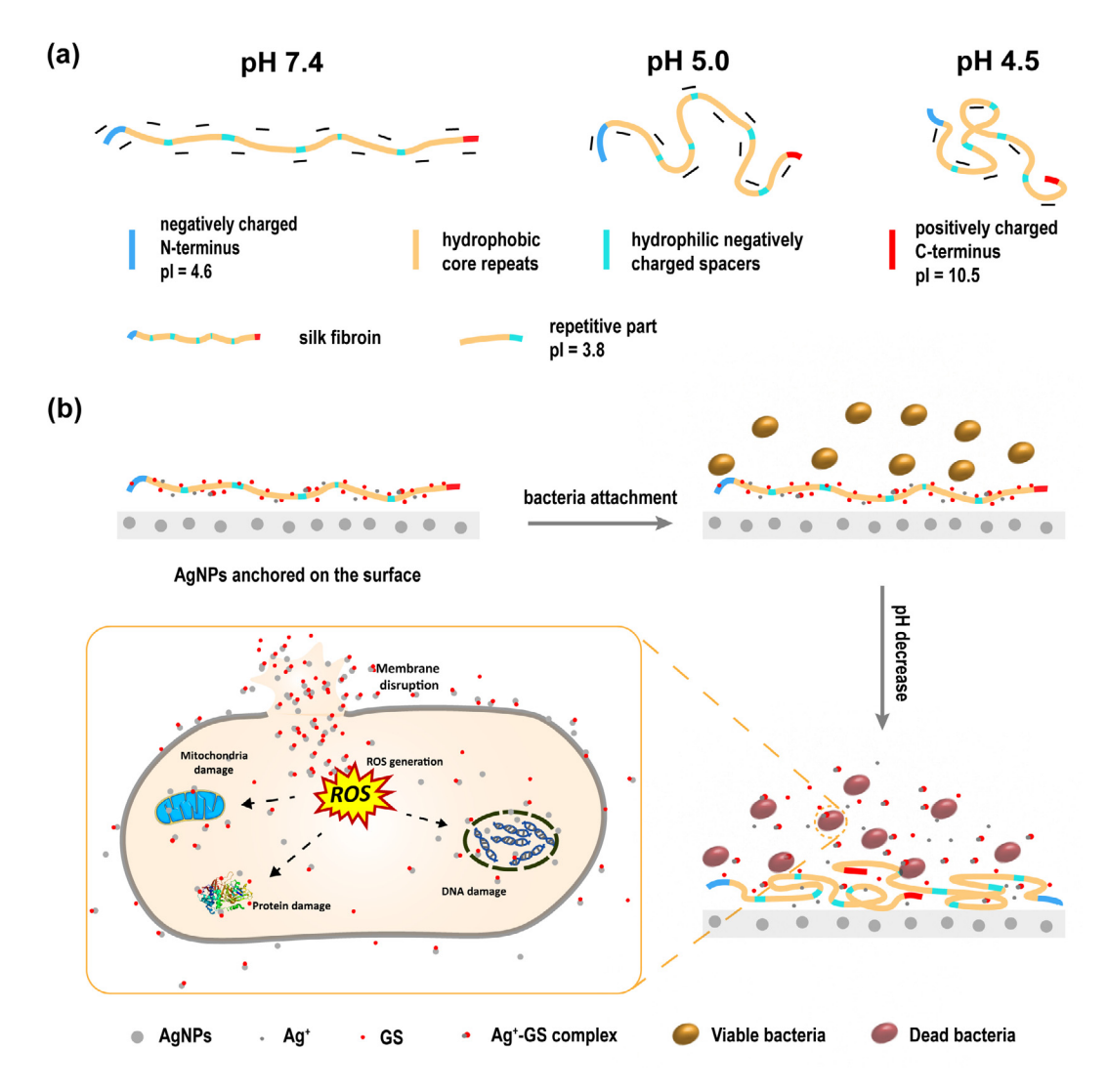


Fig. 9. Schematic illustration of the mechanism of bacteria-triggered synergistic bactericidal ability. (a) pH-responsive release mechanism of silk fibroin; (b) bacteria-triggered synergistic bactericidal process and mechanism.

What's more noteworthy, Ag⁺ and GS presented a pHresponsive release behavior, as faster and larger amount release of Ag⁺ and GS was achieved under lower pH conditions. pH is a relevant stimulus for antibacterial coatings since many bacteria metabolically acidify their local environment. In particular, S. aureus and E. coli produce lactic and acetic acid, respectively [54,55]. In this point, it was fair to say a coating with bacteria-triggered selfdefensive ability was constructed on SP-PDA-Ag/GS-Silk sample. This coating achieved the delivery of therapeutic agents only when and where needed, so unnecessary premature elution of bactericide could be controlled. Such unnecessary release puts pressure on bacteria to develop antibiotic resistance, as suboptimal concentration of bactericide has been considered as a crucial aspect of the antibiotic resistance crisis [56,57]. Hence, this coating would be beneficial to orthopedic implants. In fact, the pH-responsive release behavior could account for the accelerated oxygen dependent dissolution of Ag+ from AgNPs due to the decrease of pH [58], and also could originate from the properties of silk fibroin (Fig. 9a). Silk fibroin consists of heavy (H) and light (L)-chain, and the H-chain involves three domains with different isoelectric point (pI): N-terminus (pI = 4.6), C-terminus (pI = 10.5), and repetitive part (pI = 3.8) [23]. Because of the difference in pI, the charge condition of three domains will be different. When exposed to physiological pH (pH = 7.4), negatively charge will be dominant in silk fibroin, and will be favorable for positively charged Ag+ and GS to form an electrostatic interaction with silk. As environment pH decreases, protonation degree of silk fibroin enhanced, followed by an accumulation of positive amino groups. It brings about an imbalance between negative and positive charges and results in the release of positively charged Ag⁺ and GS to maintain electroneutrality at lower pH values. On the other hand, pHresponsive release behavior can also be governed by conformation change of silk fibroin. Specifically, when exposed to a solution of pH 7.4, all amino acid side chains except the C-terminus are negatively charged eliciting a rather elongated molecular conformation due to repulsive charge-charge interaction along the biopolymer backbone [23]. Thus, all of these negatively charged groups can be exposed to positively charged Ag+ and GS. As pH decreases, the repulsive interactions along the silk are suppressed, resulting in a less extended and more compact conformation. Therefore, fewer negatively charged groups are exposed outside, leading to release of Ag⁺ and GS. Because of the control of electrostatic interaction and conformation, silk would be a promising material that can be used to control the release of bactericide in a pHresponsive manner. Also important, the released dose of bactericide is determined by the degree of pH lowering that is associated with the metabolic activity of bacteria.

This synergistic bactericidal approach could also be detrimental to the host cell adhesion and impair implant integration due to the toxicity of Ag⁺. Actually, the directly employed of AgNPs did harm cell adhesion, proliferation, and also osteogenesis (Fig. 8). However, after being coated with silk fibroin, the specimen displayed a significant enhancement in cytocompatibility and osteogenic ability. Silk fibroin had made a great contribution to it. First, silk fibroin acted as a barrier that prevented the direct contact between AgNPs and cell membrane and also slowed down the release rate of Ag⁺, so as to relieved the toxicity of silver. Second, silk fibroin increased the contact angle from 42.5° to 56°, which would be better for cell adhesion [59,60]; meanwhile, the adsorption amount of BSA protein was increased due to the increased hydrophobic interaction, electrostatic interaction, and also hydrogen bonding between silk and BSA protein. Noteworthily, the protein adsorbed on biomaterial surface influences the adhesion of cells, to some extent governs the cell attachment [61]. On the other hand, the enhanced osteogenic ability also originated from the similar structure between silk fibroin and collagen type I [62,63].

This novel coating did endow PEEK implant with bacteriatriggered synergistic bactericidal ability. Moreover, good cytocompatibility and osteogenesis were also achieved. PEEK material with this dual functions coating would be a promising material for orthopedic implants to combat against BAI. More importantly, this coating can be applied to virtually any type and shape of implants/ devices, thanks to the capability of PDA to form robust and strong adhesion to virtually all types of substrates and the inherent wetchemical nature of treatments. However, there has a different perspective about cytocompatibility of the treated samples. It said that the cytocompatibility comparison should be done among treated group and SP group (not PEEK group) as the bulk material was completely different after sulfonate treatment. In that case, SP-PDA-Ag/GS-Silk group showed compromised cytocompatibility compared with SP group (Fig. 8a, b). Especially for the cell proliferation, at least 50% cytotoxicity was shown in the first 5 days compared with the SP group, and was alleviated on the seventh day. Actually, this perspective revealed the disadvantage of this coating, which was the insufficient of cytocompatibility. Therefore, more work should focus on improving the cytocompatibility of this material. In addition, more studies should be conducted to further investigate the effectiveness of this coating in vivo and clinical.

5. Conclusions

In this study, a mussel inspired, AgNPs incorporated SF/GS coating was constructed upon porous PEEK surface. The resultant coating presented a smart bacteria-triggered synergistic bacteria-killing ability while improving the ability of cell adhesion, proliferation, and osteogenesis. This dual functions of this coating can guarantee the victory of the cells in the "race for the surface", thus holding great promise for engineering bacteria-resistant biomedical implants.

6. Conflict of interest

The authors indicated no potential conflict of interest.

Acknowledgments

This work is jointly supported by National Natural Science Foundation of China (No. 31670974, No. 31370954).

Appendix A. Supplementary data

Supplementary data associated with this article can be found, in the online version, at https://doi.org/10.1016/j.actbio.2018.08.037.

References

- [1] J. Raphel, M. Holodniy, S.B. Goodman, S.C. Heilshorn, Multifunctional coatings to simultaneously promote osseointegration and prevent infection of orthopaedic implants, Biomaterials 84 (2016) 301–314.
- [2] S.N. Qasim, A. Swann, R. Ashford, The DAIR (debridement, antibiotics and implant retention) procedure for infected total knee replacement - a literature review, SICOT J. 3 (2017) 2.
- [3] H.J. Busscher, H.C. Van Der Mei, G. Subbiahdoss, P.C. Jutte, J.J.A.M. Van Den Dungen, S.A.J. Zaat, M.J. Schultz, D.W. Grainger, Biomaterial-associated infection: Locating the finish line in the race for the surface, Sci. Transl. Med. 4 (2012), 153rv10.
- [4] D. Campoccia, L. Montanaro, C.R. Arciola, A review of the biomaterials technologies for infection-resistant surfaces, Biomaterials 34 (2013) 8533– 8554.
- [5] D. Campoccia, L. Montanaro, C.R. Arciola, A review of the clinical implications of anti-infective biomaterials and infection-resistant surfaces, Biomaterials 34 (2013) 8018–8029.
- [6] S. Daghighi, J. Sjollema, H.C. van der Mei, H.J. Busscher, E.T. Rochford, Infection resistance of degradable versus non-degradable biomaterials: an assessment of the potential mechanisms, Biomaterials 34 (2013) 8013–8017.

- [7] S. Chernousova, M. Epple, Silver as antibacterial agent: ion, nanoparticle, and metal, Angew. Chem. Int. Ed. Engl. 52 (2013) 1636–1653.
- [8] B. Le Ouay, F. Stellacci, Antibacterial activity of silver nanoparticles: a surface science insight, Nano Today 10 (2015) 339–354.
- [9] G. Wang, W. Jin, A.M. Qasim, A. Gao, X. Peng, W. Li, H. Feng, P.K. Chu, Antibacterial effects of titanium embedded with silver nanoparticles based on electron-transfer-induced reactive oxygen species, Biomaterials 124 (2017) 25–34.
- [10] A. Gupta, K. Matsui, J.F. Lo, S. Silver, Molecular basis for resistance to silver cations in Salmonella, Nat. Med. 5 (1999) 183–188.
- [11] K. Mijnendonckx, N. Leys, J. Mahillon, S. Silver, R. Van Houdt, Antimicrobial silver: uses, toxicity and potential for resistance, Biometals 26 (2013) 609– 621.
- [12] J. RubenMorones-Ramirez, J.A. Winkler, C.S. Spina, J.J. Collins, Silver enhances antibiotic activity against gram-negative bacteria, Sci. Transl. Med. 5 (2013). 190ra81.
- [13] Y. Yang, H.Y. Ao, S.B. Yang, Y.G. Wang, W.T. Lin, Z.F. Yu, T.T. Tang, In vivo evaluation of the anti-infection potential of gentamicin-loaded nanotubes on titania implants, Int. J. Nanomed. 11 (2016) 2223–2234.
- [14] S.M. Kurtz, J.N. Devine, PEEK biomaterials in trauma, orthopedic, and spinal implants, Biomaterials 28 (2007) 4845–4869.
- [15] D. Almasi, N. Iqbal, M. Sadeghi, I. Sudin, M.R. Abdul Kadir, T. Kamarul, Preparation methods for improving PEEK's bioactivity for orthopedic and dental application: a Review, Int. J. Biomater. (2016, 2016,) 1–12.
- [16] T.J. Webster, A.A. Patel, M.N. Rahaman, B. Sonny Bal, Anti-infective and osteointegration properties of silicon nitride, poly(ether ether ketone), and titanium implants, Acta Biomater. 8 (2012) 4447–4454.
- [17] L. Ouyang, Y. Zhao, G. Jin, T. Lu, J. Li, Y. Qiao, C. Ning, X. Zhang, P.K. Chu, X. Liu, Influence of sulfur content on bone formation and antibacterial ability of sulfonated PEEK, Biomaterials 83 (2016) 115–126.
- [18] W. Zhang, Y. Yao, N. Sullivan, Y. Chen, Modeling the primary size effects of citrate-coated silver nanoparticles on their ion release kinetics, Env. Sci. Technol. 45 (2011) 4422–4428.
- [19] P. Rivero, J. Goicoechea, I. Matias, F. Arregui, A comparative study of two different approaches for the incorporation of silver nanoparticles into layerby-layer films, Nanoscale Res. Lett. 9 (2014) 1–11.
- [20] H. Lee, S.M. Dellatore, W.M. Miller, P.B. Messersmith, Mussel-inspired surface chemistry for multifunctional coatings, Science 318 (2007) 426–430.
- [21] Y. Liu, K. Ai, L. Lu, Polydopamine and its derivative materials: synthesis and promising applications in energy, environmental, and biomedical fields, Chem. Rev. 114 (2014) 5057–5115.
- [22] F.P. Seib, G.T. Jones, J. Rnjak-Kovacina, Y. Lin, D.L. Kaplan, pH-Dependent anticancer drug release from silk nanoparticles, Adv. Healthc. Mater. 2 (2013) 1606–1611.
- [23] A.S. Lammel, X. Hu, S.H. Park, D.L. Kaplan, T.R. Scheibel, Controlling silk fibroin particle features for drug delivery, Biomaterials 31 (2010) 4583–4591.
- [24] B. Kundu, R. Rajkhowa, S.C. Kundu, X. Wang, Silk fibroin biomaterials for tissue regenerations, Adv. Drug Deliv. Rev. 65 (2013) 457–470.
- [25] J. Melke, S. Midha, S. Ghosh, K. Ito, S. Hofmann, Silk fibroin as biomaterial for bone tissue engineering, Acta Biomater. 31 (2016) 1–16.
- [26] Y. Zhao, H.M. Wong, W. Wang, P. Li, Z. Xu, E.Y.W. Chong, C.H. Yan, K.W.K. Yeung, P.K. Chu, Cytocompatibility, osseointegration, and bioactivity of three-dimensional porous and nanostructured network on polyetheretherketone, Biomaterials 34 (2013) 9264–9277.
- [27] Y.B. Lee, Y.M. Shin, J.H. Lee, I. Jun, J.K. Kang, J.C. Park, H. Shin, Polydopamine-mediated immobilization of multiple bioactive molecules for the development of functional vascular graft materials, Biomaterials 33 (2012) 8343–8352.
- [28] W. Zhou, Z. Jia, P. Xiong, J. Yan, Y. Li, M. Li, Y. Cheng, Y. Zheng, Bioinspired and biomimetic AgNPs/gentamicin-embedded silk fibroin coatings for robust antibacterial and osteogenetic applications, ACS Appl. Mater. Interfaces 9 (2017) 25830–25846.
- [29] D.N. Rockwood, R.C. Preda, T. Yücel, X. Wang, M.L. Lovett, D.L. Kaplan, Materials fabrication from *Bombyx mori* silk fibroin, Nat. Protoc. 6 (2011) 1612–1631.
- [30] J. Gubernator, Z. Drulis-Kawa, A. Kozubek, A simply and sensitive fluorometric method for determination of gentamicin in liposomal suspensions, Int. J. Pharm. 327 (2006) 104–109.
- [31] C.N. Lok, C.M. Ho, R. Chen, Q.Y. He, W.Y. Yu, H. Sun, P.K. Tam, J.F. Chiu, C.M. Che, Proteomic analysis of the mode of antibacterial action of silver nanoparticles, J. Proteome Res. 5 (2006) 916–924.
- [32] Z. Jia, P. Xiu, M. Li, X. Xu, Y. Shi, Y. Cheng, S. Wei, Y. Zheng, T. Xi, H. Cai, Z. Liu, Bioinspired anchoring AgNPs onto micro-nanoporous TiO₂ orthopedic coatings: trap-killing of bacteria, surface-regulated osteoblast functions and host responses, Biomaterials 75 (2016) 203–222.
- [33] M. Pino, N. Stingelin, K.E. Tanner, Nucleation and growth of apatite on NaOHtreated PEEK, HDPE and UHMWPE for artificial cornea materials, Acta Biomater. 4 (2008) 1827–1836.
- [34] H. Doğan, T.Y. Inan, M. Koral, M. Kaya, Organo-montmorillonites and sulfonated PEEK nanocomposite membranes for fuel cell applications, Appl. Clay Sci. 52 (2011) 285–294.
- [35] X. Hu, K. Shmelev, L. Sun, E.S. Gil, S.H. Park, P. Cebe, D.L. Kaplan, Regulation of silk material structure by temperature-controlled water vapor annealing, Biomacromolecules 12 (2011) 1686–1696.

- [36] M.M. Nasef, H. Saidi, Surface studies of radiation grafted sulfonic acid membranes: XPS and SEM analysis, Appl. Surf. Sci. 252 (2006) 3073–3084.
- [37] J.J. Foti, B. Devadoss, J.A. Winkler, J.J. Collins, G.C. Walker, Oxidation of the guanine nucleotide pool underlies cell death by bactericidal antibiotics, Science 336 (2012) 315–319.
- [38] S. Bakhshandeh, Z. Gorgin Karaji, K. Lietaert, A.C. Fluit, C.H.E. Boel, H.C. Vogely, T. Vermonden, W.E. Hennink, H. Weinans, A.A. Zadpoor, S. Amin, Yavari, Simultaneous delivery of multiple antibacterial agents from additively manufactured porous biomaterials to fully eradicate planktonic and adherent staphylococcus aureus, ACS Appl. Mater. Interfaces 9 (2017) 25601–25699
- [39] N. Xu, H. Cheng, J. Xu, F. Li, B. Gao, Z. Li, C. Gao, K. Huo, J. Fu, W. Xiong, Silver-loaded nanotubular structures enhanced bactericidal efficiency of antibiotics with synergistic effect in vitro and in vivo, Int. J. Nanomed. 12 (2017) 731–743.
- [40] M. Lorenzetti, I. Dogsa, T. Stosicki, D. Stopar, M. Kalin, S. Kobe, S. Novak, The influence of surface modification on bacterial adhesion to titanium-based substrates, ACS Appl. Mater. Interfaces 7 (2015) 1644–1651.
- [41] A.M. Gallardo-Moreno, M.A. Pacha-Olivenza, L. Saldana, C. Perez-Giraldo, J.M. Bruque, N. Vilaboa, M.L. Gonzalez-Martin, In vitro biocompatibility and bacterial adhesion of physico-chemically modified Ti6Al4V surface by means of UV irradiation, Acta Biomater. 5 (2009) 181–192.
- [42] F. Hamadi, H. Latrache, H. Zahir, A. Elghmari, M. Timinouni, M. Ellouali, The relation between Escherichia coli surface functional groups' composition and their physicochemical properties, Braz. J. Microbiol. 39 (2008) 10–15.
- [43] W.L. Du, S.S. Niu, Y.L. Xu, Z.R. Xu, C.L. Fan, Antibacterial activity of chitosan tripolyphosphate nanoparticles loaded with various metal ions, Carbohydr. Polym. 75 (2009) 385–389.
- [44] Z.M. Xiu, Q.B. Zhang, H.L. Puppala, V.L. Colvin, P.J.J. Alvarez, Negligible particle-specific antibacterial activity of silver nanoparticles, Nano Lett. 12 (2012) 4271–4275.
- [45] L. Rizzello, P.P. Pompa, Nanosilver-based antibacterial drugs and devices: mechanisms, methodological drawbacks, and guidelines, Chem. Soc. Rev. 43 (2014) 1501–1518.
- [46] M.A. Kohanski, D.J. Dwyer, J.J. Collins, How antibiotics kill bacteria: from targets to networks, Nat. Rev. Microbiol. 8 (2010) 423–435.
- [47] M.A. Kohanski, D.J. Dwyer, B. Hayete, C.A. Lawrence, J.J. Collins, A common mechanism of cellular death induced by bactericidal antibiotics, Cell 130 (2007) 797–810.
- [48] Q.L. Feng, J. Wu, G.Q. Chen, F.Z. Cui, T.N. Kim, J.O. Kim, A mechanistic study of the antibacterial effect of silver ions on Escherichia coli and Staphylococcus aureus, J. Biomed. Mater. Res. 52 (2000) 662–668.
- [49] A.V. Vargiu, H. Nikaido, Multidrug binding properties of the AcrB efflux pump characterized by molecular dynamics simulations, Proc. Natl. Acad. Sci. U.S.A. 109 (2012) 20637–20642.
- [50] J.M. Blair, M.A. Webber, A.J. Baylay, D.O. Ogbolu, L.J. Piddock, Molecular mechanisms of antibiotic resistance, Nat. Rev. Microbiol. 13 (2015) 42–51.
- [51] Y.-W. Wang, H. Tang, D. Wu, D. Liu, Y. Liu, A. Cao, H. Wang, Enhanced bactericidal toxicity of silver nanoparticles by the antibiotic gentamicin, Environ. Sci. Nano 3 (2016) 788–798.
- [52] K. Zheng, M.I. Setyawati, T.P. Lim, D.T. Leong, J. Xie, Antimicrobial cluster bombs: silver nanoclusters packed with daptomycin, ACS Nano 10 (2016) 7934–7942.
- [53] M.A. Borovinskaya, R.D. Pai, W. Zhang, B.S. Schuwirth, J.M. Holton, G. Hirokawa, H. Kaji, A. Kaji, J.H. Cate, Structural basis for aminoglycoside inhibition of bacterial ribosome recycling, Nat. Struct. Mol. Biol. 14 (2007) 727–732.
- [54] C. Charlier, M. Cretenet, S. Even, Y. Le Loir, Interactions between *Staphylococcus aureus* and lactic acid bacteria: an old story with new perspectives, Int. J. Food Microbiol. 131 (2009) 30–39.
- [55] K.B. Andersen, K. Von Meyenburg, Are growth rates of *Escherichia coli* in batch cultures limited by respiration?, J Bacteriol. 144 (1980) 114–123.
- [56] D.I. Andersson, D. Hughes, Microbiological effects of sublethal levels of antibiotics, Nat. Rev. Microbiol. 12 (2014) 465–478.
- [57] M.A. Kohanski, M.A. DePristo, J.J. Collins, Sublethal antibiotic treatment leads to multidrug resistance via radical-induced mutagenesis, Mol. Cell 37 (2010) 311–320.
- [58] A.M. Mittelman, A. Taghavy, Y.G. Wang, L.M. Abriola, K.D. Pennell, Influence of dissolved oxygen on silver nanoparticle mobility and dissolution in water-saturated quartz sand, J. Nanopart. Res. 15 (2013) 1–13.
- [59] C.C. Barrias, M.C. Martins, G. Almeida-Porada, M.A. Barbosa, P.L. Granja, The correlation between the adsorption of adhesive proteins and cell behaviour on hydroxyl-methyl mixed self-assembled monolayers, Biomaterials 30 (2009) 307–316.
- [60] L.C. Xu, C.A. Siedlecki, Effects of surface wettability and contact time on protein adhesion to biomaterial surfaces, Biomaterials 28 (2007) 3273–3283.
- [61] K.G. Neoh, X. Hu, D. Zheng, E.T. Kang, Balancing osteoblast functions and bacterial adhesion on functionalized titanium surfaces, Biomaterials 33 (2012) 2813–2822.
- [62] S. Midha, S. Murab, S. Ghosh, Osteogenic signaling on silk-based matrices, Biomaterials 97 (2016) 133–153.
- [63] J.R. Vetsch, S.J. Paulsen, R. Muller, S. Hofmann, Effect of fetal bovine serum on mineralization in silk fibroin scaffolds, Acta Biomater. 13 (2015) 277–285.